A State-Space Approach for Detecting Stress from Electrodermal Activity

Dilranjan S. Wickramasuriya, *Student Member, IEEE,* Chaoxian Qi, *Student Member, IEEE,*
Rose T. Faghih, *Member, IEEE*

***Abstract*— The human body responds to neurocognitive stress in multiple ways through its autonomic nervous system. Increases in heart rate, salivary cortisol and skin conductance level are often observed accompanying high levels of stress. Stress can also take on different forms including emotional, cognitive and motivational. While a precise definition for stress is lacking, a pertinent issue is to quantify the state of psychological stress manifested in the nervous system. State-space models have previously been applied to estimate an unobserved neural state (e.g. learning, consciousness) from physiological signal measurements and data collected during behavioral experiments. In this paper, we relate stress to the probability that a phasic driver impulse occurs in skin conductance signals. We apply state-space modeling to extracted binary measures to continuously track a stress level across episodes of cognitive and emotional stress as well as relaxation. Results demonstrate a promising approach for tracking stress through wearable devices.**

I. Introduction

Stress, dubbed the "Health Epidemic of the 21st Century" by the World Health Organization, involves a state of emotional arousal, unpleasantness and loss of control [1]. Stress has been linked to an increased risk of cardiovascular disease and loss of work productivity [2], [3]. It affects autonomic nervous system activity and changes in physiological signals often accompany stressful time periods [4].

Sweat gland secretions primarily serve a thermoregulation purpose. The secretions naturally cause a change in the skin's electrical conductance. A skin conductance signal typically comprises of a slow-varying tonic component and a more rapidly fluctuating phasic part. This phasic part is usually modeled as the convolution between a driver impulse train and a bi-exponential impulse response function (IRF) [5]. Individual skin conductance responses (SCRs) can be isolated by convolving a specific driver peak with the IRF. The relationship between stress and skin conductance has been attested to in multiple studies [4]. Significant changes in different skin conductance features have been observed during experiments meant to elicit stress in participants. The stressful episodes have included arithmetic tasks, the Stroop test (a color-word association task having conflicting and non-conflicting word associations), simulated tasks in human-computer interaction, viewing affective pictures and bursts of white noise [6], [7], [8], [9], [10].

There has also been considerable interest in wearable devices and body sensor networks for continuous stress monitoring. Features extracted from skin conductance signals include statistics such as the mean, median, standard deviation etc. as well as measures such peak arrival rates and amplitudes. Several different supervised learning techniques including logistic regression, support vector machines, discriminant analysis and nearest neighbor classifiers have been explored for identifying stress [11], [12], [13].

While the appearance of SCRs accompany arousal events, non-specific SCRs unrelated to arousal or stress are also visible in skin conductance data. We develop a state-space model that characterizes stress as the probability that a SCR impulse occurs. Hence, in this formulation, we represent the SCR events as point process observations. To perform maximum likelihood estimation, we use the expectation maximization (EM) algorithm to estimate the state-space model from point process data [14]. We finally express an ideal observer's certainty level as an indicator of psychological stress.

TABLE I: SUBJECT INFORMATION

Participant	Subject ID	Age	Gender	Body Mass Index $\left[\frac{kg}{m^2}\right]$
1	1	30	M	30.00
2	5	30	M	24.75
3	8	27	M	19.32
4	9	25	M	21.70
5	12	32	F	20.20
6	16	24	M	16.66

II. Methods

A. Dataset 1 - Cognitive and Emotional Stress Induced in a Laboratory Setting

We used de-identified skin conductance signals from the Non-EEG Dataset for Assessment of Neurological Status [15] [16]. In the experiment, data was collected from 20 participants who were subject to physical, cognitive and emotional stress. In this paper, we focus solely on psychological stress and exclude the physical stress period (comprising of standing, walking and jogging). Cognitive stress was induced through an arithmetic task and the Stroop test, while subjects were made to watch a clip from a horror movie for eliciting emotional stress. The arithmetic task involved counting backwards in 7s beginning at 2485. Moreover, during the cognitive stress period, a buzzer alerted subjects of any mistakes. Each major stress episode lasted for about 5 min. and had a 5 min. relaxation time in-between. The investigators later pointed out how the subjects appeared to show signs of stress even while being given instructions

D. S. Wickramasuriya, C. Qi and R. T. Faghih are with the Department of Electrical and Computer Engineering at the University of Houston, Houston, TX 77004 USA (e-mail:{dswickramasuriya, cqi4, rtfaghih}@uh.edu). This work was partly supported by NSF 1755780.

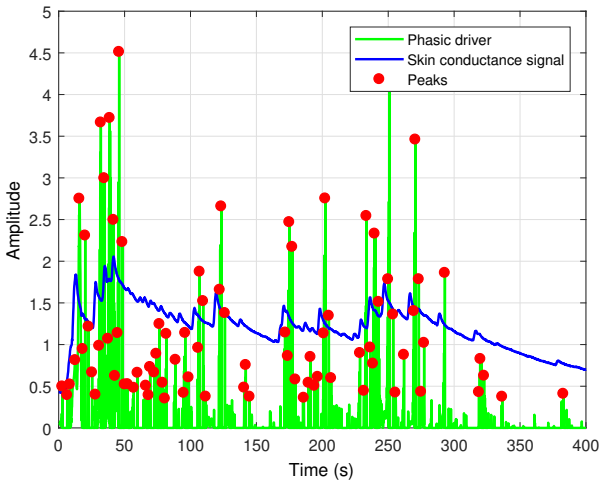

Fig. 1: **Peak detection from skin conductance signal.** The skin conductance signal (blue curve), phasic driver (green) and selected phasic driver peaks (red dots) for the recording from participant 1 in Dataset 1.

about the cognitive tasks, and hence the 40 sec period just prior to that was labeled as one of mini emotional stress.

Motion artifacts, changes in amplification factor, and range saturation can easily corrupt skin conductance signals [4]. Owing to contamination, we discarded data from 14 of the 20 subjects. Information regarding the selected subjects is provided in Table I and we refer to them as participant 1 - 6 hereafter, instead of by subject ID. We used cvxEDA [17] to obtain the phasic driver impulse train from the skin conductance data chosen for our analysis. Since the impulse train resulting from this decomposition detects small impulses that might be due to noise, we used MATLAB's *findpeaks* function to select dominant spike locations with constraints placed on the minimum amplitude and distance between consecutive peaks to minimize noise effects (Fig. 1). A further issue is that bursts of neuronal activity stimulating the sweat glands cannot occur in quick succession.

B. Dataset 2 - Driver Stress

We also used the Stress Recognition in Automobile Drivers Dataset [18] for validating our method in a real-world stressful situation. This dataset contains recordings for 17 separate drives on a set route in Boston with highways, toll roads and city driving. The drives were all conducted during the mid-morning or mid-afternoon having light traffic. Each drive began and ended with approximately 15 min. rest periods where the drivers sat in the car with their eyes shut. Since annotations indicating the start and end of each portion (i.e., rest, highway, toll road etc.) are not publicly available, we could only used one record (Fig. 2) whose approximate timings had to be matched with a figure in [18].

C. State-Space Model of Stress

We divided the time axis into bins of 1 sec duration and modeled the extracted phasic driver peaks as a point process. Each bin is assigned 1 or 0 depending on whether or not a peak appears within it. Using a state-space model of point process observations [14], we track the cognitive stress level across the entire signal. The state-space model consists of a state equation that describes the latent stress level and an observation equation describing how observed peaks are related to the state. We assume that a Gaussian state equation describes this unobserved cognitive state and a Bernoulli probability model describes the occurrence of a peak in each bin. In this study, we perform our analysis from an ideal observer's perspective (i.e., someone who has already seen the entire signal), and estimate stress at each bin based on detected peaks.

We set the total number of bins K and index them as $k = 1, 2, ..., K$ in our state-space model. For the observation equation, we use s_k to denote a peak detected in bin k, where s_k follows a Bernoulli distribution, ($s_k = 1$ represents a peak in bin k, and $s_k = 0$ otherwise). We define q_k as the probability that a peak occurs in bin k. For the state equation, we let z_k denote an unobserved stress level. Variations in skin conductance are closely related to stress and thus the probability q_k depends on z_k. Given a value of the state process z_k, the observation model defines the probability of observing s_k. Similar to [14], the observation model can be described using the Bernoulli distribution as follows:

$$P(s_k|q_k) = q_k^{s_k}(1 - q_k)^{1-s_k} \tag{1}$$

where q_k is defined by a logistic equation:

$$q_k = \frac{1}{1 + e^{-(\alpha + z_k)}} \tag{2}$$

The parameter α is related to the random chance that a peak occurs in a bin at the start of the experiment. We set $z_0 = 0$, and calculate α using (2) taking $q_0 = 0.1155$ as the empirically determined chance probability that a peak occurs in a bin. We define the evolution of the stress state as a random walk:

$$z_k = z_{k-1} + \epsilon_k \tag{3}$$

where $\epsilon_k \sim \mathcal{N}(0, \sigma_\epsilon^2)$.

We observe $S_{1:K} = \{s_1, s_2, ..., s_K\}$ indicating the presence or absence of peaks. The objective is to estimate $Z = \{z_0, z_1, z_2, ..., z_K\}$ and σ_ϵ^2 for in turn estimating $q_k \ \forall k$. As z is unobserved and σ_ϵ^2 is a parameter, we use the EM algorithm to estimate z and σ_ϵ^2 [14]. The E-step consists of a point process recursive nonlinear filter algorithm and a fixed-interval smoothing algorithm. The M-step maximizes the expected value of the complete data log likelihood [14].

D. Stress State Estimation

In the E-step, the filter algorithm computes the state estimate of the subject and the smoothing algorithm calculates the estimate of the ideal observer. The filter algorithm estimates $z_{k|k}$ in bin k, given $S_{1:k}$, the data up to bin k with the true parameter σ_ϵ^2 replaced by its maximum likelihood estimate. The fixed-interval smoothing algorithm estimates $z_{k|K}$ at bin k, given $S_{1:K}$, all the data in the experiment with

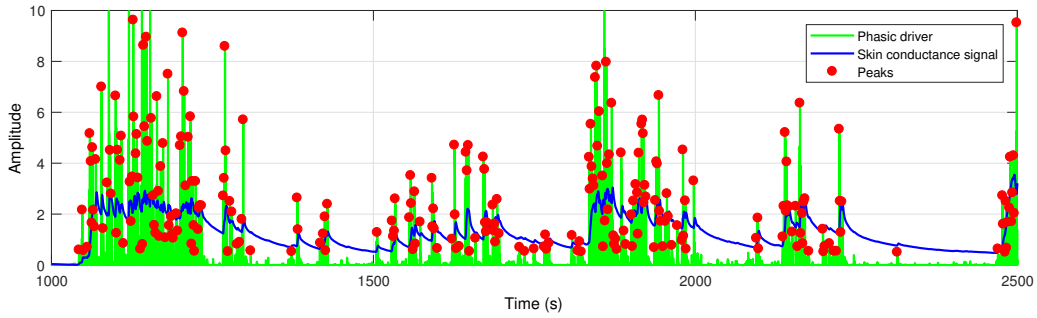

Fig. 2: **Peak detection from skin conductance signal.** The skin conductance signal (blue curve), phasic driver (green) and selected phasic driver peaks (red dots) for the hand skin conductance signal in drive R2-1 [18] in Dataset 2.

the true parameter σ_ϵ^2 replaced by its maximum likelihood estimate. The filter algorithm estimates the stress state in bin k as a Gaussian random variable with mean $z_{k|k}$ and variance $\sigma_{k|k}^2$ whereas the smoothing algorithm does so with mean $z_{k|K}$ and variance $\sigma_{k|K}^2$. We make a Gaussian approximation in the filter formulation although strictly the point process nature of the observations is non-Gaussian. We let $q_{k|k}$ denote the probability of a peak occurring in bin k given the data $S_{1:k}$ up to bin k, and $q_{k|K}$ the probability of a peak in bin k given all of the data $S_{1:K}$. This EM variation for estimating the state-space model from point process observations is summarized below.

E. Expectation Step

At iteration $(l+1)$ of the algorithm, we compute the expectation of all the data log likelihood in the E-step given $S_{1:K}$, the stress state, $\sigma_\epsilon^{2(l)}$ and $z_0^{(l)}$, which are the parameter estimates from iteration l.

Forward Filter: We estimate state variable $z_{k|k}$ and its variance $\sigma_{k|k}^2$, given $\sigma_\epsilon^{2(l)}$ and $z_0^{(l)}$, using a recursive non-linear filter algorithm [14]. This algorithm is based on a derivation of maximizing posterior probability of the Kalman filter algorithm [19], [20]. The filter algorithm is given as follows:

$$z_{k|k-1} = z_{k-1|k-1} \tag{4}$$

$$\sigma_{k|k-1}^2 = \sigma_{k-1|k-1}^2 + \sigma_\epsilon^{2(l)} \tag{5}$$

$$z_{k|k} = z_{k|k-1} + \sigma_{k|k-1}^2 \left[s_k - \frac{1}{1+e^{-(\alpha+z_{k|k})}} \right] \tag{6}$$

$$\sigma_{k|k}^2 = \left\{ \frac{1}{\sigma_{k|k-1}^2} + \frac{e^{(\alpha+z_{k|k})}}{[1+e^{(\alpha+z_{k|k})}]^2} \right\}^{-1} \tag{7}$$

for $k = 1, 2, ..., K$. The initial condition is $z_0 = z_0^{(l)}$ and $\sigma_{0|0}^2 = \sigma_\epsilon^{2(l)}$. $z_{k|k}$ appears on both sides of (6) and this nonlinear equation can be solved using Newton's method.

Backward Filter: From (6) and (7), we can obtain the posterior mode estimate $z_{k|k}$ and its variance $\sigma_{k|k}^2$. Given this data, we apply the fixed-interval smoothing algorithm to compute $z_{k|K}$ and $\sigma_{k|K}^2$. The fixed interval smoothing algorithm is given as follows [14]:

$$A_k = \frac{\sigma_{k|k}^2}{\sigma_{k+1|k}^2} \tag{8}$$

$$z_{k|K} = z_{k|k} + A_k \left(z_{k+1|K} - z_{k+1|k} \right) \tag{9}$$

$$\sigma_{k|K}^2 = \sigma_{k|k}^2 + A_k^2 \left(\sigma_{k+1|K}^2 - \sigma_{k+1|k}^2 \right) \tag{10}$$

for $k = K-1, ..., 1$. The initial conditions are $z_{K|K}$ and $\sigma_{K|K}^2$.

F. Maximization Step

The expected value of the complete data likelihood is maximized as follows [14]:

$$\begin{aligned} \sigma_\epsilon^{2(l+1)} = \frac{2}{K+1} \Bigg[& \sum_{k=2}^{K} (\sigma_{k|K}^2 + z_{k|K}^2) \\ & - \sum_{k=2}^{K} (A_k \sigma_{k|K} + z_{k|K} z_{k-1|K}) \Bigg] \\ & + \frac{1}{K+1} \left[\frac{3}{2} (\sigma_{1|K}^2 + z_{1|K}^2) - (\sigma_{K|K}^2 + z_{K|K}^2) \right] \end{aligned} \tag{11}$$

$$z_0^{(l+1)} = \frac{1}{2} z_{1|K} \tag{12}$$

Notations $z_{k|j}$, $\sigma_{k|j}^2$, and $q_{k|j}$, respectively, denote the stress state, its variance and the probability of a peak occurring in bin k. The algorithm iterates between the E-step and the M-step in two loops until convergence. The change of variables formula can be applied to the Gaussian probability density with mean $z_{k|j}$ and variance $\sigma_{k|j}^2$ to obtain the probability density for q_k using the forward $(j = k)$ or backward $(j = K)$ filter algorithms as follows [14]:

$$\begin{aligned} f(q|\alpha, z_{k|j}, \sigma_{k|j}^2) = & \frac{1}{\sqrt{2\pi\sigma_{k|j}^2} q(1-q)} \\ & \times \exp\left\{ \frac{-1}{2\sigma_{k|j}^2} \left[-z_{k|j} + \log \frac{q}{(1-q)e^\alpha} \right]^2 \right\} \end{aligned} \tag{13}$$

From (12), we can compute confidence intervals similar to [14] to obtain the ideal observer's assessment regarding

the probability that the appearance of a peak in bin k was more than just due to chance (i.e., due instead to stress).

III. Results

A. Dataset 1

Estimates for $q_{k|k}$, $q_{k|K}$ and the ideal observer's certainty level of stress for the six participants in Dataset 1 are shown in Fig. 3. Participant 1 appears to be stressed out considerably during the cognitive stress portion of the experiment (recall that the mini emotional stress period at the outset was actually when participants were receiving directions about the cognitive tasks). His stress level drops significantly during the relaxation period that follows and increases momentarily at the start of the horror movie. Since the $q_{k|k}$ and $q_{k|K}$ values are extremely low at the end of the experiment, the corresponding confidence intervals can be seen to span the entire support of q_k in $[0, 1]$. Participant 2 is also visibly stressed during the cognitive tasks based on the ideal observer's certainty assessment. Stress level can also be seen to decline since the start of the horror movie. There is one notable exception in that there is a significant momentary increase right in the middle of the relaxation period. The stress profile of participant 3 also follows the typical pattern of being high during cognitive stress, dropping significantly during relaxation and having a short increase that eventually dies out since the start of the horror movie. An exception is noted here again with a momentary increase, though not exceeding 90%, towards the end of the movie clip.

Participant 4 has a somewhat varied response in comparison to the others. While increases are noted during cognitive stress, the 90% certainty threshold is only exceeded towards the end of the Stroop test. Stress level also remains higher for slightly longer than usual into the relaxation period. Reaction to the horror movie is somewhat similar and two initial stress responses over the 90% certainty threshold gradually decline with time. In the case of participant 5, stress level remains high almost constantly during the cognitive tasks. It drops significantly during relaxation and remains very low during the horror movie with two slight increases. The stress profile for participant 6 is typical as well, similar to that of participants 1 and 3.

B. Dataset 2

Stress estimates for the driver are shown in Fig. 4. Except for a short spike in stress during the initial rest period, the subject appears to be relatively calm from the ideal observer's perspective until driving commences. While exact traffic condition annotations are unavailable for each different period, the subject's stress level can only be seen to drop significantly for reasonable lengths of time during highway driving (yellow). City driving (blue) and driving on the toll roads (red) is stressful to the subject. Somewhat surprising is the fact that the subject appears remarkably stressed, almost comparable to when driving, during the second rest period at the conclusion of the route. This exception has been elaborated on in the following section.

IV. Discussion and Conclusion

Stress responses to similar stimuli and associated psychophysiology vary between different individuals. State-space modeling has the advantage of being able to pick up some of the subtle differences among subjects when exposed to cognitive and emotional stress. In Dataset 1, all participants were seen to have a high level of stress during the cognitive tasks. Both the arithmetic task and Stroop test involved active cognitive engagement and added the stress of alerting the subjects of any mistakes with a buzzer. In contrast, watching the horror movie only involved passive engagement. Skin conductance signals in general are known to be sensitive to psychological arousal [4]. It is likely that an initial to stress response or excitement at the start of the horror movie gradually wore off as the clip proceeded.

Driving can be a stressful experience and Dataset 2 affords the opportunity to analyze stress in a real-world situation. The subject's stress level varies considerably during the entire route. No clear changes exist between city driving and driving on the toll roads or highways. Without actual traffic annotations or self-reported scores, it is difficult to correlate the stress level fluctuations within each type of road condition to anything more specific. In [18], a stress metric was calculated for the duration of the drive based on collected data. Concering the particular subject in drive R2-1, the authors in [18] note "During this drive, the subject was unusually agitated during the second rest period due to a need to use the restroom [and] this agitation is reflected in the stress metric." This confirms the high stress level noted in our analysis too during the latter rest period.

This paper presented a state-space model for recovering a stress level from phasic driver impulses in skin conductance signals. The model was evaluated on publicly available datasets with signals recorded from subjects during different stressful scenarios, both artificially induced and real-world. Although not expressly calculated here, the percentage of time the ideal's observer's certainty level exceeds 90% would be a suitable stress metric to be incorporated into a wearable device. We plan to extend the deconvolution strategy in [21] to recover the amplitudes of the sparse phasic driver impulses and include these values in our state-space model. Incorporating additional physiological measures, such as heart rate, to supplement this analysis would enable a broader system capable of quantifying both psychological valence and arousal [4]. We could also extend the work by using particle filters for non-linear state estimation [22].

The EM algorithm must be executed offline for parameter estimation. Stress estimation could therefore be executed batchwise once every 5 min. or so, or the EM algorithm could be run at predefined intervals for optimal parameter selection and just the filter algorithm be used for tracking stress in-between.

References

[1] G. Fink, "Chapter 1 - stress, definitions, mechanisms, and effects outlined: Lessons from anxiety," in *Stress: Concepts, Cognition, Emotion, and Behavior*, pp. 3 – 11, San Diego: Academic Press, 1st ed., 2016.

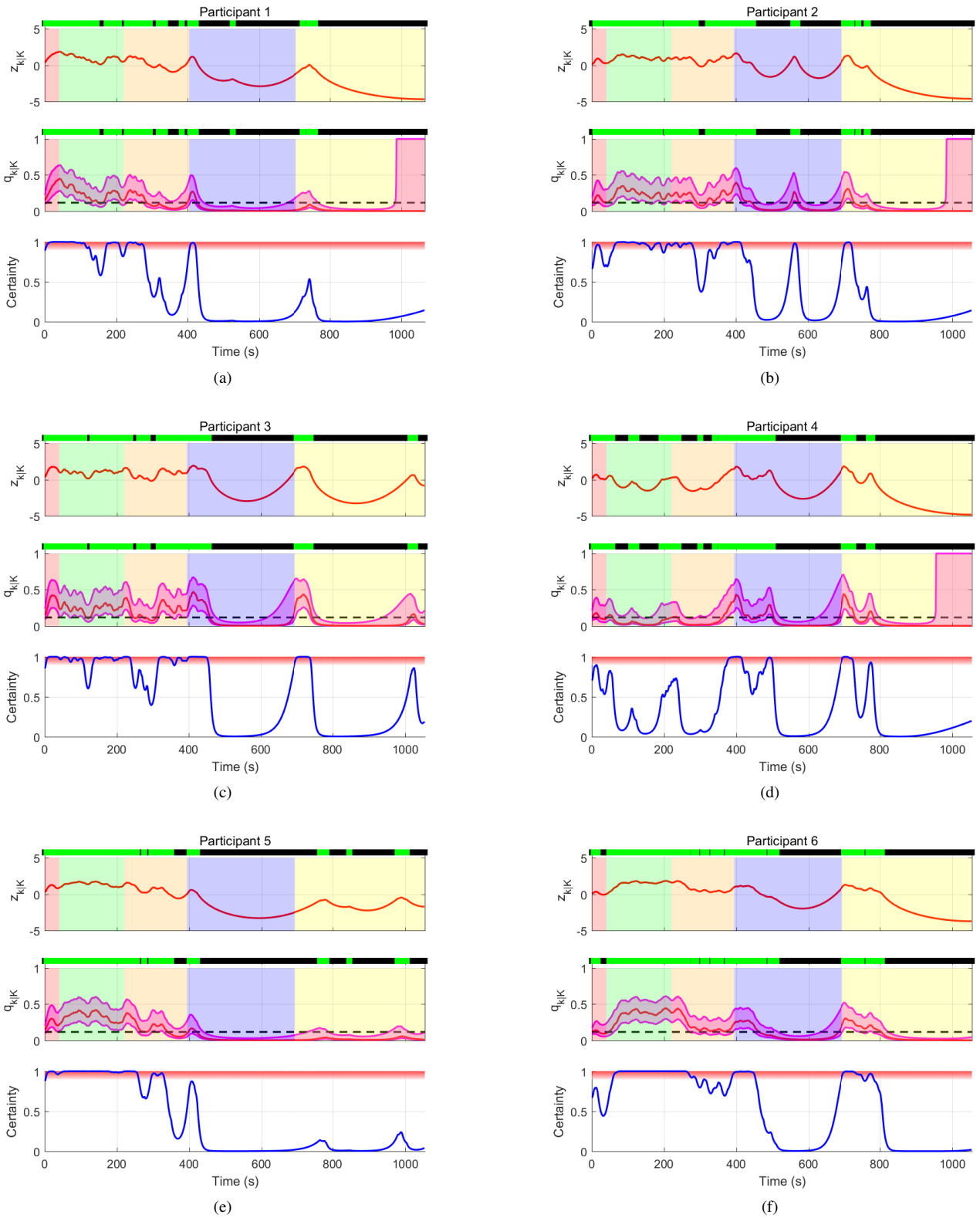

Fig. 3: **Stress state estimation.** In each figure panel, (i) the top sub-panel depicts $z_{k|K}$; (ii) the middle sub-panel depicts $q_{k|K}$ and its confidence intervals; (iii) the lower sub-panel depicts the observer's certainty level of stress with the region above 90% highlighted in red for participants in Dataset 1. The color-coded backgrounds correspond to mini emotional stress, the arithmetic task, the Stroop test (both forming cognitive stress), relaxation and emotional stress. Green dots above both upper sub-panels depict peak locations.

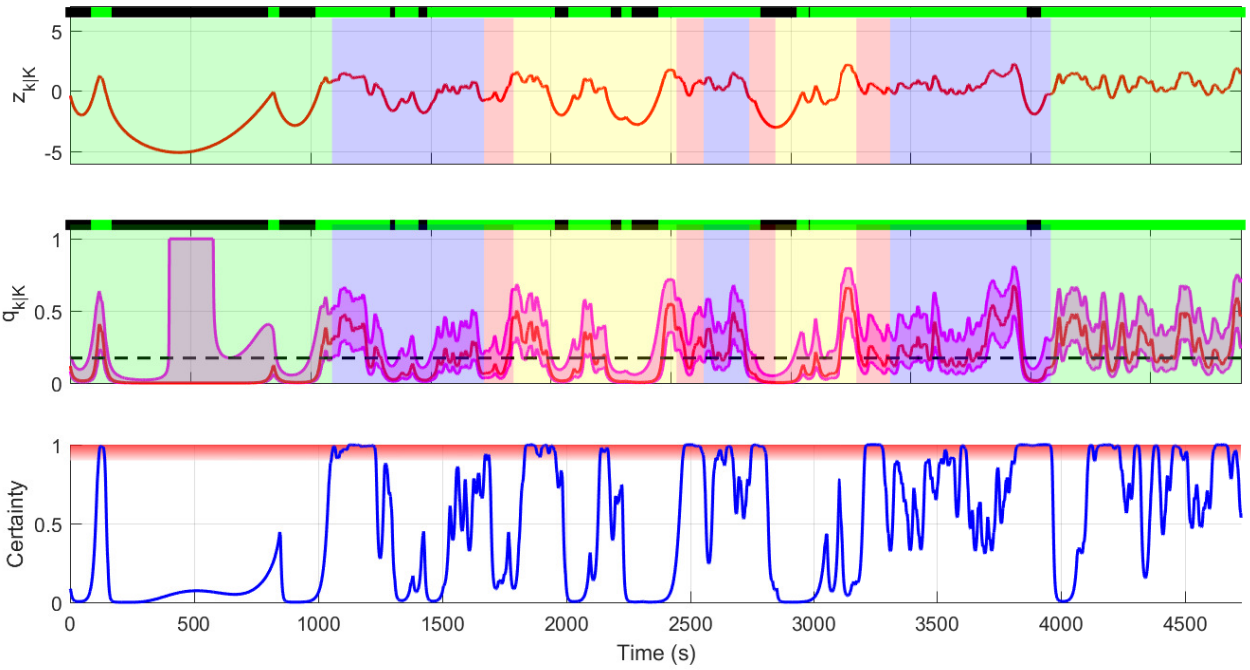

Fig. 4: **Stress state estimation.** The upper sub-panels depict $z_{k|K}$ and $q_{k|K}$ with its confidence intervals. The lower sub-panel depicts the observer's certainty level of stress for the subject in Dataset 2. The color-coded backgrounds correspond in turn to rest, city driving, toll road, highway, toll road, city driving, toll road, highway, toll road, city driving and rest.

[2] S. A. Everson-Rose and T. T. Lewis, "Psychosocial factors and cardiovascular diseases," *Annu. Review of Public Health*, vol. 26, pp. 469–500, 2005.

[3] T. W. Colligan and E. M. Higgins, "Workplace stress: Etiology and consequences," *J. Workplace Behavioral Health*, vol. 21, no. 2, pp. 89–97, 2006.

[4] W. Boucsein, *Electrodermal Activity*. New York, NY: Springer Science & Business Media, 2nd ed., 2012.

[5] M. Benedek and C. Kaernbach, "Decomposition of skin conductance data by means of nonnegative deconvolution," *Psychophysiology*, vol. 47, no. 4, pp. 647–658, 2010.

[6] Z. Visnovcova, M. Mestanik, M. Gala, A. Mestanikova, and I. Tonhajzerova, "The complexity of electrodermal activity is altered in mental cognitive stressors," *Comput. Biology and Medicine*, vol. 79, pp. 123–129, 2016.

[7] M. Svetlak, P. Bob, M. Cernik, and M. Kukleta, "Electrodermal complexity during the Stroop colour word test," *Autonomic Neuroscience*, vol. 152, no. 1, pp. 101–107, 2010.

[8] H. F. Posada-Quintero, J. P. Florian, Á. D. Orjuela-Cañón, and K. H. Chon, "Highly sensitive index of sympathetic activity based on time-frequency spectral analysis of electrodermal activity," *Amer. J. Physiology-Regulatory, Integrative and Comparative Physiology*, vol. 311, no. 3, pp. R582–R591, 2016.

[9] A. Liapis, C. Katsanos, D. Sotiropoulos, M. Xenos, and N. Karousos, "Recognizing emotions in human computer interaction: studying stress using skin conductance," in *Human-Comput. Interaction*, pp. 255–262, Springer, 2015.

[10] T. Reinhardt, C. Schmahl, S. Wüst, and M. Bohus, "Salivary cortisol, heart rate, electrodermal activity and subjective stress responses to the Mannheim multicomponent stress test (MMST)," *Psychiatry Research*, vol. 198, no. 1, pp. 106–111, 2012.

[11] A. Sano and R. W. Picard, "Stress recognition using wearable sensors and mobile phones," in *Humaine Assoc. Conf. Affective Comput. and Intell. Interaction (ACII), 2013*, pp. 671–676, IEEE, 2013.

[12] J. Choi, B. Ahmed, and R. Gutierrez-Osuna, "Development and evaluation of an ambulatory stress monitor based on wearable sensors," *IEEE Trans. Inf. Technol. Biomed.*, vol. 16, no. 2, pp. 279–286, 2012.

[13] C. Setz, B. Arnrich, J. Schumm, R. La Marca, G. Tröster, and U. Ehlert, "Discriminating stress from cognitive load using a wearable EDA device," *IEEE Trans. Inf. Technol. Biomed.*, vol. 14, no. 2, pp. 410–417, 2010.

[14] A. C. Smith, L. M. Frank, S. Wirth, M. Yanike, D. Hu, Y. Kubota, A. M. Graybiel, W. A. Suzuki, and E. N. Brown, "Dynamic analysis of learning in behavioral experiments," *J. Neuroscience*, vol. 24, no. 2, pp. 447–461, 2004.

[15] J. Birjandtalab, D. Cogan, M. B. Pouyan, and M. Nourani, "A non-EEG biosignals dataset for assessment and visualization of neurological status," in *IEEE Int. Workshop Signal Process. Syst. (SiPS)*, pp. 110–114, 2016.

[16] A. L. Goldberger, L. A. N. Amaral, L. Glass, J. M. Hausdorff, P. C. Ivanov, R. G. Mark, J. E. Mietus, G. B. Moody, C.-K. Peng, and H. E. Stanley, "PhysioBank, PhysioToolkit, and PhysioNet: Components of a new research resource for complex physiologic signals," *Circulation*, vol. 101, pp. e215–e220, June 2000.

[17] A. Greco, G. Valenza, A. Lanata, E. P. Scilingo, and L. Citi, "cvxEDA: A convex optimization approach to electrodermal activity processing," *IEEE Trans. Biomed. Eng.*, vol. 63, no. 4, pp. 797–804, 2016.

[18] J. A. Healey and R. W. Picard, "Detecting stress during real-world driving tasks using physiological sensors," *IEEE Trans. Intell. Transp. Syst.*, vol. 6, no. 2, pp. 156–166, 2005.

[19] J. M. Mendel, *Lessons in Estimation Theory for Signal Processing, Communications, and Control*. Pearson Education, 1995.

[20] E. N. Brown, L. M. Frank, D. Tang, M. C. Quirk, and M. A. Wilson, "A statistical paradigm for neural spike train decoding applied to position prediction from ensemble firing patterns of rat hippocampal place cells," *J. Neuroscience*, vol. 18, no. 18, pp. 7411–7425, 1998.

[21] R. T. Faghih, P. A. Stokes, M.-F. Marin, R. G. Zsido, S. Zorowitz, B. L. Rosenbaum, H. Song, M. R. Milad, D. D. Dougherty, E. N. Eskandar, and R. Barbieri, "Characterization of fear conditioning and fear extinction by analysis of electrodermal activity," in *37th Annu. Int. Conf. IEEE Eng. Medicine and Biology Society (EMBC)*, pp. 7814–7818, IEEE, 2015.

[22] T. B. Schön, A. Wills, and B. Ninness, "System identification of nonlinear state-space models," *Automatica*, vol. 47, no. 1, pp. 39–49, 2011.